

An experimental and numerical study of parasitic capillary waves

Alexey V. Fedorov,^{a)} W. Kendall Melville, and Anatol Rozenberg

Scripps Institution of Oceanography, University of California San Diego, La Jolla, California 92093-0230

(Received 6 October 1997; accepted 20 February 1998)

We report laboratory measurements of nonlinear parasitic capillary waves generated by longer waves in a channel. The experiments are conducted for three frequencies of longer waves (4, 5, and 6 Hz), corresponding to wavelengths of approximately 11, 7, and 5 cm. For these wavelengths we apply a model developed recently by Fedorov and Melville [J. Fluid Mech. **354**, 1 (1998)] to predict the wave profile. Based on a viscous boundary layer approximation near the surface, the model enables us to efficiently calculate gravity-capillary waves. We present direct comparisons that show good agreement between the measurements and numerical predictions over a range of parameters. Finally, we give some simple estimates for a sharp cutoff in the wave number spectra observed in both the numerical solutions and the laboratory measurements of short gravity-capillary waves.

© 1998 American Institute of Physics. [S1070-6631(98)01206-9]

I. INTRODUCTION

The generation of parasitic capillary waves (or parasitic capillaries) by steep gravity-capillary waves is an important mechanism for momentum, energy, and gas transfer between the atmosphere and ocean. The effects of gravity and surface tension determine the fine structure of the ocean surface, which is important for microwave remote sensing of the ocean. Experimental research on parasitic capillary waves has a relatively long history, including pioneering work by Cox¹ and subsequent studies^{2,3} that have provided temporal measurements of the surface slope of mechanically or wind-generated waves at a single location. Ebuchi *et al.*⁴ produced high-quality images of wind-generated gravity-capillary waves with distinct trains of parasitic capillaries riding ahead of bulging wave crests. They argued that the crest of such waves (the ‘‘capillary roller’’⁵) is a region of high vorticity in the water. Jähne and Riemer⁶ (1990), among others,⁷⁻⁹ have used various optical techniques to measure the local slope of gravity-capillary waves and to deduce wave number spectra.

Perlin *et al.*¹⁰ presented spatial measurements of plunger-generated waves with parasitic capillaries. Regrettably, their results were strongly affected by the fact that they took measurements within a few wavelengths of the wave generator.¹¹ Perlin *et al.* also tried to compare their measurements with theoretical results available at that time, including the analytical models of Longuet-Higgins (1963)¹² and several others.^{13,14} Their comparisons gave large quantitative, and even qualitative, departures from these theories. Ruvinsky *et al.*¹⁵ developed a new theory and compared some of their results with those by Yermakov *et al.*³ However, they were able to reproduce parasitic capillaries of only very low amplitudes, and their comparisons lacked important details.

Better qualitative and quantitative agreement with the available experiments was achieved by the theory of Longuet-Higgins (1995),¹¹ who introduced a new perturbation model for steady gravity-capillary waves. The underlying longer wave was assumed to be a pure gravity wave given by a Stokes expansion, which served as the first approximation for the model. Surface tension and the large curvature of the crest of the gravity wave acted as a local forcing term, leading to the excitation of parasitic capillaries by a mechanism analogous to the ‘‘fish line’’ problem.¹⁶ The main limitation of Longuet-Higgins’ theory was that parasitic capillary waves appeared only as a linear response to the forcing.

Recently, Fedorov and Melville¹⁷ have developed a new theory capable of describing nonlinear gravity-capillary waves. The theory is based on a viscous boundary layer approximation near the surface, and uses a full Stokes expansion with complex coefficients, which reflects the asymmetry of the wave profile. It also includes external forcing necessary to balance the viscous dissipation. A preliminary comparison with experiments showed good agreement between the model and limited experimental data. In this study we carry out a more extensive set of measurements to further test our theoretical results.¹⁷

We also discuss the nature of the so-called ‘‘high-wavenumber cut off’’^{17,6,9} (an abrupt decrease by several orders of magnitude) in the spectral energy density after the spectral maximum corresponding to capillary ripples (Sec. V). We provide some simple estimates for calculating the bandwidth of the main capillary maximum, as well as the cutoff wave number.

II. ANALYTICAL MODEL AND NUMERICAL APPROACH

For completeness, the theoretical model and numerical approach of Fedorov and Melville¹⁷ are reviewed here. To treat periodic surface waves of permanent form, we transform to a frame of reference traveling with speed c to the

^{a)}Current address: AOS program, Princeton University, P.O. Box CN710, Sayre Hall, Princeton, New Jersey 08544.

right ($c > 0$). In this reference frame the motion is steady. Following the classical boundary layer approximation, we assume that the flow is irrotational everywhere except in a thin subsurface viscous boundary layer. We also adopt the assumption of classical linear damping.¹⁷⁻¹⁹ It implies that all Fourier harmonics of the wave are damped independently, while higher-order nonlinear dissipative terms can be neglected.

Irrotational flow is used to describe the gravity-capillary waves in the first approximation. Then additional terms due to the presence of the viscous boundary layer are calculated, modifying the original irrotational variables. Accordingly, Bernoulli's integral for the surface of the weakly damped flow is derived, while a Stokes expansion with complex coefficients is used to represent the surface waves. External pressure forcing, which is needed for the waves to remain steady and periodic, is explicitly included in the model.

Using this approach we formulate a closed set of equations, yielding a parametric representation of the free surface,

$$X = X(\zeta), \quad Y = Y(\zeta), \tag{1}$$

or

$$Z = X + iY, \tag{2}$$

where X and Y are horizontal and vertical coordinates of the free surface, and ζ is the independent parameter. The details of the derivation are given in Ref. 17. Here we present only the final formulation: One needs to find Z^i , such that

$$Z^i = \frac{1}{k} \left(\zeta + i \sum_{m=1}^{\infty} a_m e^{-im\zeta} \right), \quad \zeta \in [0, 2\pi], \tag{3}$$

and

$$\frac{U^i{}^2}{2} + gY + \frac{T}{R} + \frac{P_0}{\rho} + \frac{\nu k}{c} \frac{\partial}{\partial \zeta} U^i{}^2 = E, \tag{4}$$

where

$$U^i = -\frac{c}{k} (Z_{\zeta}^i Z_{\zeta}^{i*})^{-1/2}, \tag{5}$$

$$Z = Z^i - \frac{2i\nu}{c^2 k} \int_0^{\zeta} \left(\frac{U^i}{R^i} - \left\langle \frac{U^i}{R^i} \right\rangle \right) d\zeta', \tag{6}$$

$$\frac{1}{R} = -\text{Im}\{Z_{\zeta}^i Z_{\zeta}^{-3/2} Z_{\zeta}^{i*}{}^{-1/2}\}, \tag{7}$$

$$P_0 = \tilde{P}_0 \cos kX, \tag{8}$$

with

$$X = \text{Re } Z - \text{Re } Z|_{\zeta=0} \quad \text{and} \quad Y = \text{Im } Z, \tag{9}$$

and

$$\frac{1}{R^i} = -\text{Im}\{Z_{\zeta}^i Z_{\zeta}^{-3/2} Z_{\zeta}^{i*}{}^{-1/2}\}, \tag{10}$$

and

$$\left\langle \frac{U^i}{R^i} \right\rangle = \frac{1}{2\pi} \int_0^{2\pi} \frac{U^i}{R^i} d\zeta'. \tag{11}$$

Here, ρ is the fluid density; g , gravity; T , the surface tension, and P_0 the external pressure forcing at the surface necessary to balance the wave dissipation. U^i , Z^i , and $1/R^i$ are the irrotational component of the flow velocity on the surface, the complex coordinate of the free surface, and the local curvature, respectively. In addition, $1/R$ is the full local curvature of the surface. Equation (3) is a Stokes expansion with as yet unknown coefficients a_m . Equation (4) is Bernoulli's integral for a steady weakly damped flow with an unknown constant E . When a_m, c and E are found, Z^i is determined from Eq. (3). After calculating Z , the elevation of the free surface is given by (9).

In addition to Eqs. (3)-(11), we introduce the dimensionless wave amplitude as

$$ak = [\max(Y) - \min(Y)]k/2, \tag{12}$$

corresponding to the characteristic slope of the wave of wave number $k = 2\pi/\lambda$. Clearly, fixing ak is necessary to specify the wave height.

For the external forcing P_0 in (4) and (8), we took a simple cosine profile, $\tilde{P}_0 \cos kx$, although more general forms may be used. The forcing is necessary to balance the dissipation and keep the waves periodic and steady. For example, the forcing may represent the surface pressure distribution due to the effect of wind on the water surface. The length scale of the forcing coincides with the wavelength of the longer wave, so that parasitic capillaries are not directly affected by the external pressure. Together with \tilde{P}_0 , we use a nondimensional amplitude of the forcing,

$$p = \tilde{P}_0 / \rho c_0^2, \tag{13}$$

where

$$c_0 = \sqrt{g/k + Tk} \tag{14}$$

is the phase speed of linear gravity-capillary waves. The solutions have a parametric dependence on λ, p , and ak .

To solve the system (1)-(14), we discretize equations on the interval of ζ from 0 to 2π and truncate them, retaining about 100 terms of the series. (More terms are needed for calculating strongly nonlinear solutions with overhanging wave crests, which are not considered in this paper.¹⁷) All the derivatives with respect to ζ are calculated using Eq. (3), and the integrals in (6) and (11) are evaluated by means of the trapezoidal rule. This procedure yields a finite set of algebraic equations in a_m, c and E , with ak, p , and the wavelength λ as independent parameters. (This is different from regular steady gravity waves, for which the wave amplitude and the wavelength are the only parameters.) The coefficient of surface tension T and viscosity ν are assumed to be fixed.

The resulting set of equations is solved numerically via Newton's method. We calculate the Jacobian for Newton's iterations numerically, rather than analytically, as in other similar studies.²⁰ As an initial guess, we usually take a profile corresponding to a linear gravity-capillary wave. In other cases, we use a previously calculated solution as the initial guess, but change the combination of parameters. The iterations converge in a broad range of ak and p . (For details see Fedorov and Melville.¹⁷)

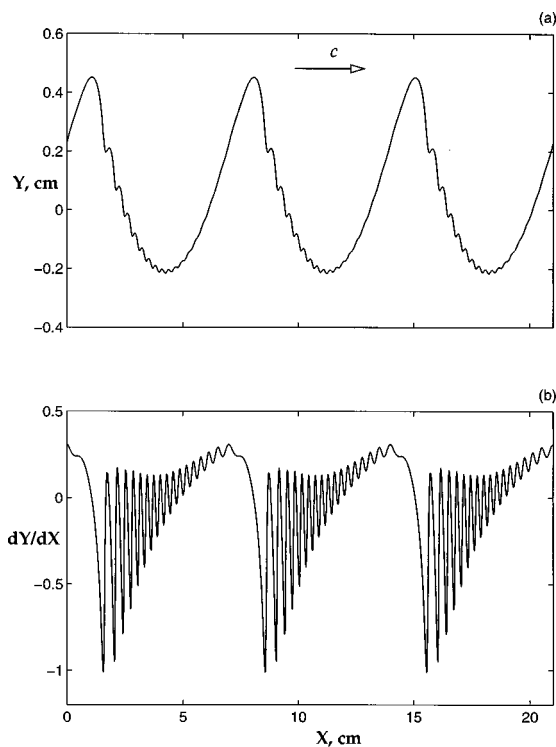


FIG. 1. An example of numerical calculations for the profile of the free surface and its slope for $\lambda = 7$ cm, $ak = 0.30$, and $p = 0.015$. Strong capillary ripples ride on longer waves. Note the different vertical and horizontal length scales in (a).

Numerical calculations and linear analysis of the system (1)–(14) show that there are two main classes of solution for weak forcing (class 1 and class 2, for $p \ll ak$). For the first class, the pressure maximum occurs near the wave trough, while for the second it is near the crest. Both types of waves are qualitatively similar, with only small quantitative differences for weak forcing. Both yield asymmetric profiles with shorter parasitic capillary waves riding on the forward face of the longer waves. An example of our solutions for the class 1 waves is shown in Fig. 1. See Figs. 6 and 7 below for comparisons of class 1 and class 2 solutions.

III. EXPERIMENTAL SETUP

Experiments were conducted in the Hydraulics Laboratory at Scripps Institution of Oceanography. A 30 m long, 0.5 m wide, and 0.6 m deep glass wave channel equipped with a wave generator was used (Fig. 2). Measurements were taken at fetches greater than 1 m away from the wave generator, which is equivalent to 10 to 20 wavelengths of the longer waves. To remove contaminants, the surface of the channel was cleaned periodically by blowing wind and skimming the surface at the downwind end of the channel. With time the surface becomes contaminated, resulting in a dramatic decrease in the amplitudes of capillary waves.

Surface waves were generated mechanically by the vertical motion of a wedge-shaped plunging wavemaker. Measurements of the surface slope were made with a fixed laser slope gauge (LSG). This device, which is designed to measure the fine structure of short water waves, consists of an

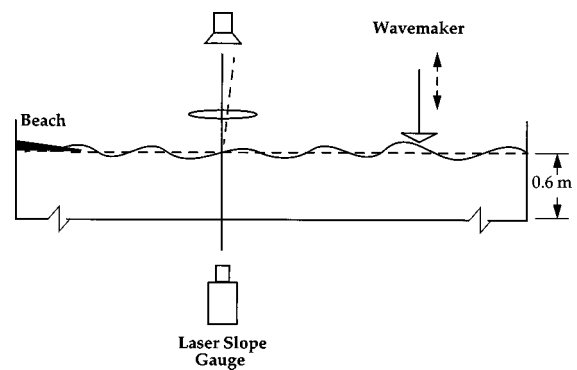


FIG. 2. Schematic of the experimental setup showing the channel, the wavemaker, and the laser slope gauge. The channel is 30 m long.

underwater laser assembly, lenses to focus the beam on a position photodiode, and a signal amplifier. The LSG uses the refraction of a laser beam^{8,21} by the water surface to measure the slope of the surface. A Fresnel lens was used to eliminate the effects of the vertical displacement of the surface on the slope measurements. A detailed description of a similar LSG can be found in Lange *et al.*,²² for example.

Data were sampled at 1 kHz, while the time series for each combination of parameters was about 30 s long. The experiments were conducted with wavemaker frequencies of 6, 5, and 4 Hz corresponding to wavelengths of approximately 5, 7, and 11 cm. The spatial resolution of the LSG was approximately 0.7 mm. The errors in the slope measurement were estimated to be in the range 5%–10%.

IV. WAVE SLOPES FOR DIFFERENT AMPLITUDES AND FREQUENCIES: EXPERIMENTAL RESULTS

In Fig. 3 we show a 5 s section of a typical time series for 5 Hz gravity-capillary waves. The higher-frequency parasitic capillaries are predominantly at the negative slopes. The wave pattern is regular and almost stationary; however, one can notice some temporal unsteadiness over times of $O(1)$ s. (A substantially less steady pattern is observed for 4 Hz waves, see Fig. 4(c) below.) A typical frequency spectrum of the slope time series is presented in Fig. 3(b). Following a monotonic decrease in amplitude up to the eighth harmonic there follows an increase in the spectral density associated with the parasitic capillaries. There is a sharp decline in the spectral energy density after this increase, or a spectral “cutoff.”^{17,6,8,9} The plot also shows a higher-order capillary maximum, which has been predicted by the theory.¹⁷

In Figs. 4(a)–4(c), we present a one-second-long time series obtained for different wave frequencies and amplitudes. First, one can notice the apparent increase in amplitude of parasitic capillaries with the increasing slope of the longer wave. The amplitude of the parasitic capillaries is rather sensitive to the amplitude of the longer waves. This is true, especially for 4 Hz waves that develop shorter capillary waves and require a greater steepness for the appearance of the ripples. Although the local wavelength of the ripples varies along the longer wave, we can estimate characteristic wavelengths of the capillary ripples from the spectrum. This

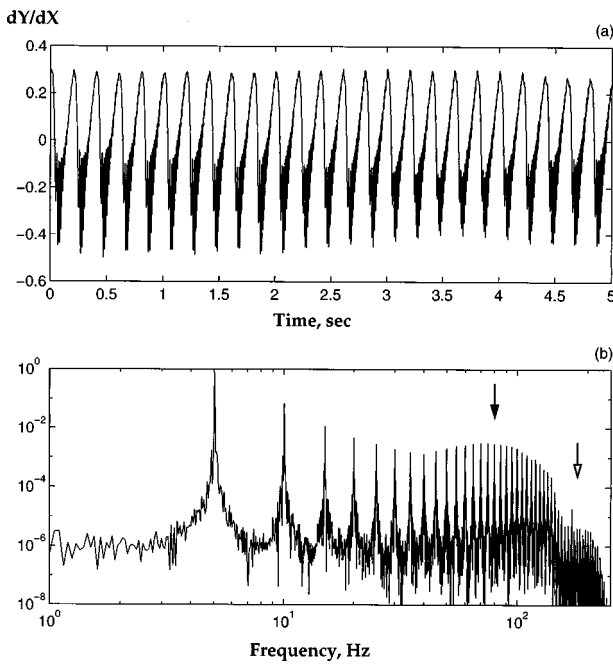


FIG. 3. The 5 Hz waves. (a) An example of a 5 s time series of the measured wave slope. The darker unresolved parts of the plot correspond to parasitic capillaries. (b) A typical frequency spectrum of the time series. Each peak to the right of 5 Hz is a harmonic of the fundamental wave. The increase in harmonic amplitudes indicated by the solid arrow corresponds to the appearance of parasitic capillaries. Note a sharp decline in the spectral energy density after this increase (the cutoff^{17,6,9}). The open arrow shows a higher-order capillary maximum, also predicted by the theory.¹⁷

gives wavelengths of approximately 6, 5, and 4 mm for 6, 5, and 4 Hz longer waves, respectively. Note that, especially in the case of the 4 Hz waves, the definition of characteristic wavelength becomes less accurate because of the widening of the capillary maximum in the spectrum.

For both 6 and 5 Hz waves, the wave patterns remain quite regular, and no visible instabilities develop. However, with increasing amplitude, 4 Hz surface waves lose stability, and capillary ripples become irregular. We believe that this is due to modulational instability of the underlying longer gravity waves at these amplitudes and wavelengths, as well as three-dimensional instabilities,²³ which could be observed in the experiments.

There is another noticeable difference between the 6 and 5 Hz waves, and the 4 Hz waves. In the case of the shorter waves (5 and 6 Hz), the capillaries appear along the entire wavelength, while for the longer 4 Hz waves they are concentrated on the forward face of the wave. This is related to the stronger decay of the shorter capillary ripples.

Figure 5 summarizes our experimental measurements of the slopes of the capillary ripples for different frequencies and slopes of the longer waves. The characteristic relative slope of the ripples is obtained by averaging the capillary waves out and subtracting the smoothed profile from the data. This gives the profile of the capillary ripples. Calculating the mean square deviation yields the characteristic slope of the ripples relative to the slope of the underlying longer wave. Within the accuracy of this approach similar data can be obtained from the numerical results.

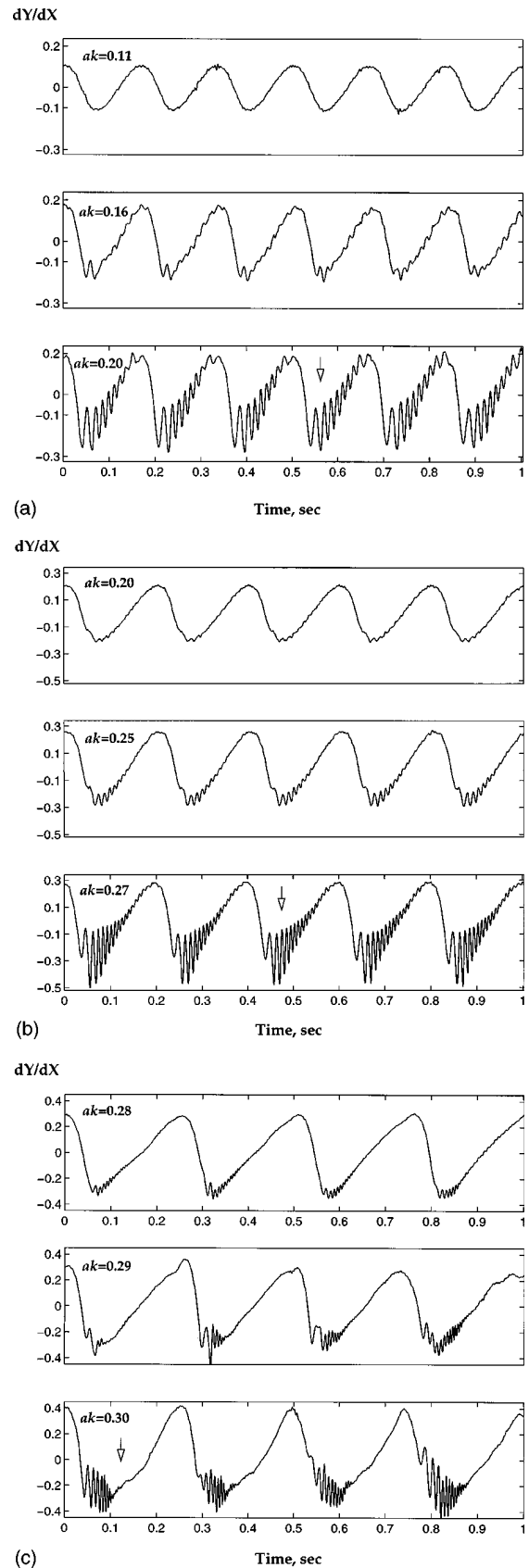


FIG. 4. Experimental measurements of the slope of mechanically generated waves in the channel for different wave amplitudes ak and frequencies. Arrows indicate the periods of the time series used for further comparison with numerical solutions (see Figs. 6, 7, and 8). The measurements are conducted for three frequencies of the dominant longer wave: (a) 6 Hz, (b) 5 Hz, (c) 4 Hz. The particular values of ak are shown in each figure.

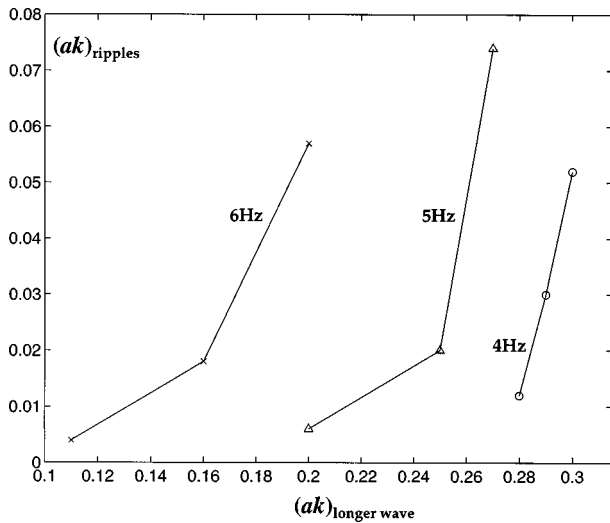


FIG. 5. The characteristic relative slope of the capillary ripples versus the slope of the underlying longer wave for different frequencies. The full local slope changes in the characteristic range of $(ak)_{\text{longer wave}} \pm (ak)_{\text{ripples}}$. Compiled from the data presented in Figs. 4(a)–4(c).

In treating our results in Fig. 5, one should be aware that (a) the amplitude of the capillary ripples varies along the longer wave, and (b) the characteristics of the capillary waves are very sensitive to changes in the amplitude of the longer wave and the conditions of the experiments. Nevertheless, Fig. 5 gives the typical dependence of the slope of

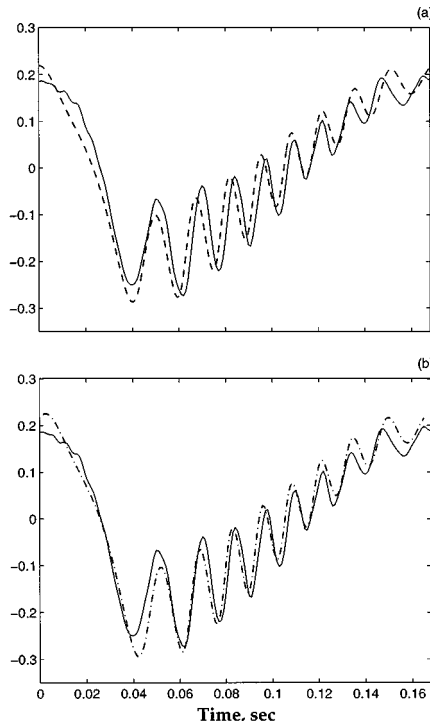


FIG. 6. Experimental measurements of the slope of 6 Hz waves (solid line), compared with numerical solutions. (a) Class 1 solution, dashed line, for $\lambda = 5.2$ cm, $ak = 0.20$, and $p = 0.0015$; (b) Class 2 solution, dot-dashed line, for $\lambda = 5.1$ cm, $ak = 0.205$, and $p = 0.005$.

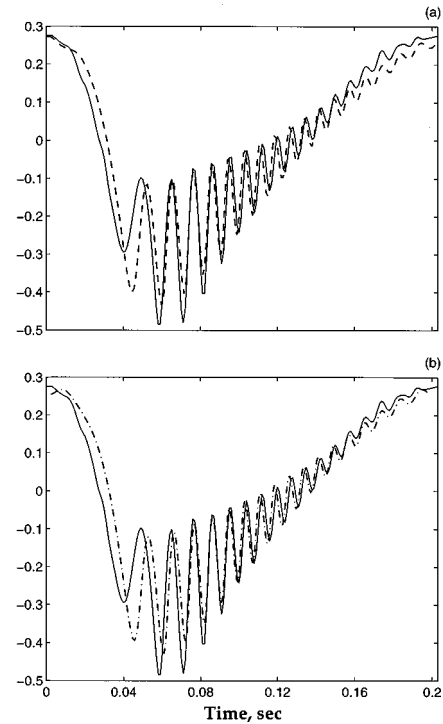


FIG. 7. Experimental measurements of the slope of 5 Hz waves (solid line), compared with numerical solutions: (a) Class 1 solution, dashed line, for $\lambda = 7.3$ cm, $ak = 0.265$, and $p = 0.0062$; (b) class 2 solution, dot-dashed line, for $\lambda = 7.1$ cm, $ak = 0.265$, and $p = 0.0014$.

the parasitic capillaries on the frequency and the slope of the longer waves. A sharp increase of the slope of the parasitic capillaries with increasing slope of the longer waves is apparent.

V. DIRECT COMPARISON OF NUMERICAL AND EXPERIMENTAL DATA. SPECTRAL CUTOFF

Before presenting a direct comparison between the numerical and experimental results, we need to note a difference between the model and experiments. In the wave channel the energy is transferred to the waves through the work of a wave generator, rather than through a pressure distribution at the surface, as in the theory. Consequently, the waves in the channel slowly decay, so that we can treat them as only quasiperiodic in space. The amplitude decay rates vary from $O(1\% - 10\%)$ per wave period depending upon the wave amplitude and frequency. This would lead to differences between the experimental measurements and theoretical predictions of the same order of magnitude (see below). However, since the error in the measurements are estimated to be in the range of 5%–10%, this should not be a leading-order effect.

A fit of the experimental results with solutions obtained numerically is shown in Fig. 6 for 6 Hz waves, and Fig. 7 for 5 Hz waves. The calculations are made for $\nu = 0.01 \text{ cm}^2 \text{ s}^{-1}$ and $T = 73 \text{ cm}^3 \text{ s}^{-2}$. The particular parts of the time series taken for comparison are indicated by arrows in Figs. 4(a), 4(b), and 4(c).

The procedure to obtain this comparison is as follows. First, we choose the appropriate value of the wavelength for numerical calculations to approximately match the frequency of the observed wave. Then we adjust the nondimensional wave amplitude ak . Finally, the value of p is changed to obtain agreement with respect to the number of capillary ripples. This procedure is repeated several times, since any change of ak and p affects the frequency of the dominant wave. When calculating the solution, we also obtain the theoretical phase speed of the wave. This enables us to present the numerical solution, as a function of time at any point of the surface.

As one can see from Figs. 6 and 7, both classes of solution provide good quantitative agreement with the observations; although we have to choose slightly different values of λ , ak , and p in each case. The number of ripples can be matched exactly, while the values of the slope differ by not more than 5% in most cases. Although a larger deviation occurs for the last ripple in the row (especially noticeable for the 5 Hz waves) the match is quite accurate. In Figs. 8(a) and 8(b) we also show a comparison between the experimental and numerical wavenumber spectra for 6 and 5 Hz waves. These are spectra of time series formed by repeating the single period used in the time-domain comparisons of Figs. 6 and 7, 64 times. This treats the waves as essentially periodic rather than quasiperiodic with subharmonic components and harmonics of finite bandwidth. The agreement between the measurements and theory is very good.

The spectra in Figs. 8(a) and 8(b) deserve some special attention. The lower wave number region of the spectra with a relatively slow decay corresponds to the first few harmonics of the fundamental wave. The first local maximum is due to parasitic capillaries. The second local maximum is associated with higher harmonics of the main capillary maximum, and is significantly weaker in magnitude. A sharp decrease in spectral density (by three to four orders of magnitude) develops after the first capillary maximum. This rapid decrease appears to be similar to the cutoff observed in the measurements of wind-wave spectra.^{6,9} We will estimate the typical wave number corresponding to the main capillary maximum and its bandwidth, which is equivalent to finding the location of the ‘‘cutoff.’’

The physical reason for the appearance of the parasitic capillaries is the amplification of higher harmonics of the fundamental waves due to a resonance. The approximate resonance condition¹ can be obtained from matching phase speeds between the longer wave (c) and the shorter capillary wave (c_c). This matching condition yields

$$c_c^2 = c^2, \tag{15}$$

or

$$Tk_c \approx \left(\frac{g}{k} + Tk \right) (1 + a^2 k^2), \tag{16}$$

where k_c is the resonant wave number of the capillary waves. For simplicity, we have disregarded the nonlinear, gravity,

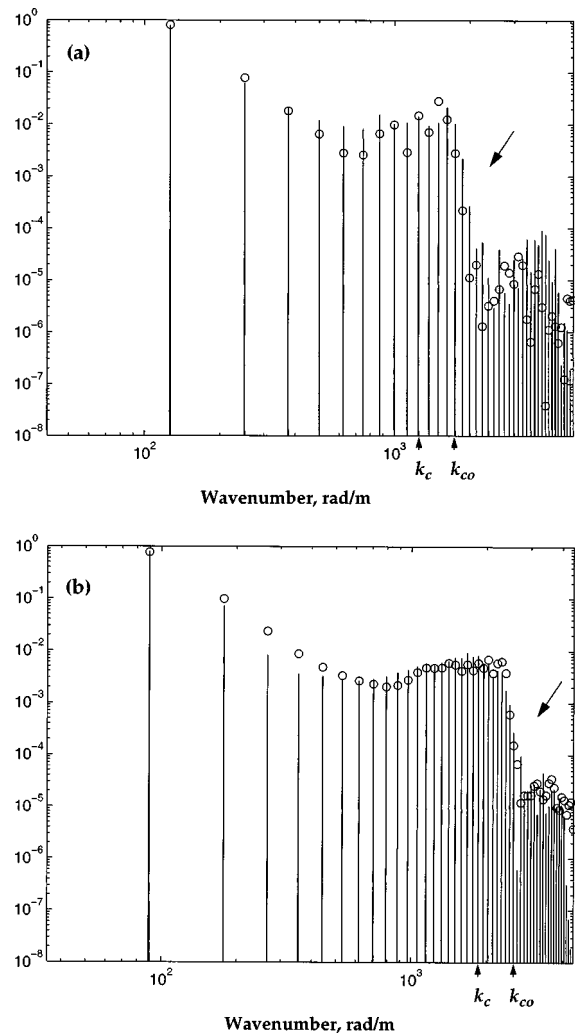


FIG. 8. The wave number spectra based on the experimental and numerical data presented in Figs. 6 and 7. The circles correspond to the spectral density obtained from the numerical calculations for the class 1 solutions. Again, notice a sharp decline in the spectral density after the main capillary maximum (the arrow). The estimated values of the resonant capillary wave number k_c and cutoff wavenumber k_{co} are shown [see Eqs. (17) and (21)]. The frequencies of the dominant longer wave are (a) 6 Hz, (b) 5 Hz.

and dissipative effects on the capillary ripples. The phase speed of the longer wave in (16) includes a nonlinear Stokes correction (Whitham, 1974).

Equation (17) gives the typical ‘‘capillary’’ wave number as

$$k_c \approx \left(\frac{g\lambda}{2\pi T} + \frac{2\pi}{\lambda} \right) (1 + a^2 k^2). \tag{17}$$

Substituting the appropriate parameters for the 6 and 5 Hz waves yields the typical wave numbers 1200 and 1700 rad/m, respectively, which falls approximately in the center of each capillary maximum in Figs. 8(a) and 8(b).

Furthermore, nonlinearity leads to the local resonant condition being different for different phases of the longer wave profile. In fact, we should match the phase speed of the capillary wave with the velocity of the local surface ‘‘cur-

rent'' induced by the longer wave. In the frame of reference moving with the wave this velocity is calculated in terms of c and ak as

$$U^2 \approx c^2(1 + 2ak \cos kX). \tag{18}$$

That is, locally, the resonant condition (16) should be replaced by

$$c_c^2 \approx c^2(1 + 2ak \cos kX). \tag{19}$$

This causes the formation of the capillary maxima with a finite bandwidth Δk_c , centered at k_c , instead of a narrow peak. Since cosine ranges from -1 to $+1$, Eq. (19) implies that

$$\frac{\Delta k_c}{k_c} \approx 4ak. \tag{20}$$

From Eq. (20), the cutoff wave number (k_{c0}) can be estimated as

$$k_{c0} = k_c + \frac{\Delta k_c}{2} = k_c(1 + 2ak). \tag{21}$$

Under this definition the cutoff wave numbers may be actually higher than in previous studies,^{15,7,10} since formula (21) provides an estimate for the uppermost limit of the main capillary maximum, rather than the beginning of the spectral falloff.

Substituting our parameters for the 6 and 5 Hz waves gives bandwidths Δk_c of about 1000 and 1800 rad/m, and the cutoff wave numbers k_{c0} about 1700 and 2600 rad/m, respectively, which is consistent with the data in Figs. 8(a) and 8(b).

The spectral cutoff appears to have a simple explanation: There is a resonant peak of finite bandwidth, after which the spectral density returns to its background values, before increasing again to reach the next, but much weaker, capillary maximum. The background values of the spectral density are much lower after the main capillary maximum because of its significant width and general decay in the spectrum. This consideration underlines the fact that the cutoff is related to the kinematics of the waves, and is not directly affected by wave dissipation as in Donelan and Pierson.²⁴

Note that in the field, wind waves have a continuous spectrum rather than a discrete spectrum determined by the fundamental wave and its harmonics. In other words, instead of one fundamental wave we may have a continuous distribution of "fundamental waves." Nevertheless, we believe that Eqs. (16) and (21) can still be used for crude estimates of the cutoff wave numbers for oceanic waves.

Finally, in Fig. 9 we present a comparison between the measurements and the theory for 4 Hz waves. We still observe good qualitative agreement, although there is no possibility of a direct comparison, since the capillary ripples are no longer stationary. An unsteady analytical formulation possibly similar to the recent work by Watson and Buchsbaum²⁵ may be useful in this case.

We have also compared the results of our calculations with calculations by Longuet-Higgins.¹¹ For moderate wave slopes our models appear to give qualitatively similar results

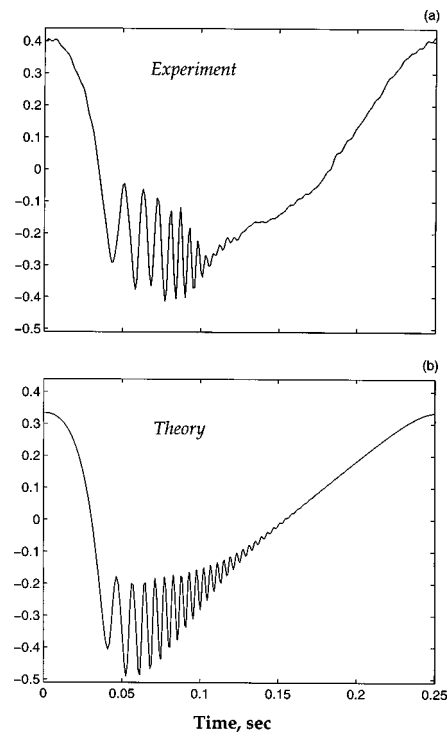


FIG. 9. Experimental measurements of the slope of 4 Hz waves (a), compared with a numerical solution (b). Calculations are for $\lambda = 11$ cm, $ak = 0.31$, and $p = 0.006$, and the class-1 solutions.

with the difference only significant for higher wave slopes and shorter wavelengths. An example of this comparison is given in the Appendix.

VI. CONCLUSIONS

The model developed by Fedorov and Melville¹⁷ is demonstrated to be in good agreement with experimental measurements over a range of parameter space. In our experiments there existed a threshold wavelength of approximately 8 cm. For smaller wavelengths the theory and measurements are in good quantitative agreement in reproducing parasitic capillary waves. Small differences can be attributed to several factors, including wave decay along the channel and errors in the measurements.

Importantly, the spectral characteristics of the measured capillary ripples are consistent with the theory. For instance, there is a cutoff (an abrupt decrease by several orders of magnitude) in the spectral energy density after the first local maximum corresponding to capillary ripples. We have deduced some simple relations providing the peak and the bandwidth of the main capillary maxima, or alternatively, the cutoff wave number.

For longer wavelengths the agreement between the theory and experiments is qualitative, possibly due to the appearance of modulational and three-dimensional instabilities of the waves, as in Zhang and Melville.²³ The instability of the dominant waves affects the shorter capillaries, making them unsteady, so that a direct comparison with a steady

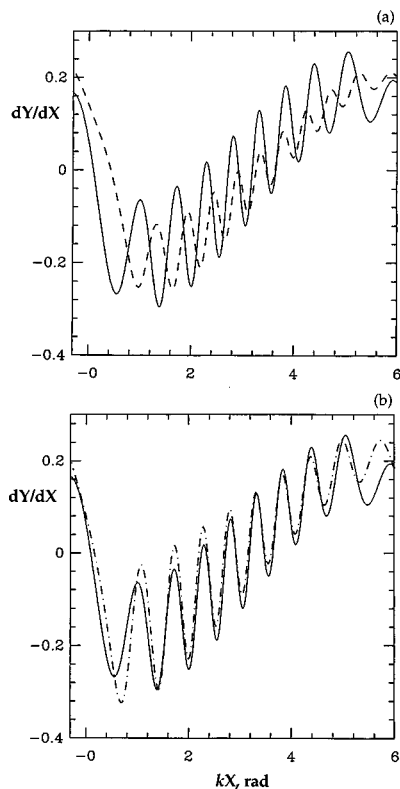


FIG. 10. A comparison between the results using our model [the class 1 solutions: (a) $p=0.001$, dashed line; (b) $p=0.02$, dash-dotted line], and those of Longuet-Higgins (1995), solid line, for $\lambda=5.5$ cm, $ak=0.199$, $T=74$ cm³ s⁻², and $\nu=0.01$ cm² s⁻¹. For weak forcing the present model yields more smaller capillary ripples. For the class 1 solutions the two methods agree better only for much stronger forcing. The agreement is significantly worse for the class 2 solutions.

model becomes impossible. However, the steady model may be used as the basis for studies of the stability of gravity-capillary waves.

ACKNOWLEDGMENTS

We thank Professor Michael Longuet-Higgins for providing the results of his calculations for 5.5 cm gravity-capillary waves. This work has been supported by a grant from the Office of Naval Research (Remote Sensing).

APPENDIX: COMPARISON WITH LONGUET-HIGGINS MODEL (1995)

We have compared the results of our calculations with those of Longuet-Higgins.¹¹ For moderate wave slopes our models appear to give qualitatively similar results, although there exist several quantitative differences. For instance, Longuet-Higgins' model usually gives fewer capillary ripples per wavelength, which is likely due to neglecting the effect of surface tension on the overall phase speed of the dominant wave. The number of ripples becomes the same only for much stronger forcing for the class 1 solutions (the agreement is significantly worse for the class-2 solutions, for which any increase of the forcing leads to weaker capillary ripples; see Fedorov and Melville¹⁷) in the model of Fedorov and Melville.¹⁷ Such strong forcing would affect the overall

phase speed of the longer wave, increasing the phase speed and resulting in shorter and stronger capillary waves.

An example of the comparison is given in Fig. 10 for 5.5 cm gravity-capillary waves (5.5 cm is the lowest wavelength of the longer waves for which Longuet-Higgins' model is still valid, which is close to our calculations for 6 Hz waves). With increasing amplitude of the longer wave the differences become larger.

Although for weaker forcing ($p=0.001$) the amplitudes of the capillaries calculated in our model (Fig. 5) are smaller than those given by Longuet-Higgins, there is no consistency as to which model gives stronger capillaries. Longuet-Higgins showed a comparison between his theory and measurements by Cox¹ for waves of approximately 5 Hz. For this particular case, our study yields more pronounced capillary ripples, both in the experimental and numerical data, which indicates the importance of nonlinearity for the parasitic capillary waves. [In contrast to our experiments for this frequency (see Sec. V), in Cox's measurements the wave height was not completely uniform and steady.] Using a linear approximation for parasitic capillaries, Longuet-Higgins' method is restricted to small capillary slopes. For example, in some cases, it may be necessary to increase the effective value of viscosity to obtain the correct values for the amplitude of the capillary ripples.

¹C. S. Cox, "Measurements of slopes of high frequency wind waves," *J. Mar. Res.* **16**, 199 (1958).

²J. H. Chang, R. N. Wagner, and H. C. Yuen, "Measurements of high frequency capillary waves on steep gravity waves," *J. Fluid Mech.* **86**, 401 (1978).

³S. A. Yermakov, K. D. Ruvinsky, S. G. Salashin, and G. I. Friedman, "Experimental investigation of the generation of capillary-gravity ripples by strongly nonlinear waves on the surface of a deep fluid," *Izv. Atmos. Ocean Phys.* **22**, 835 (1986).

⁴N. Ebuchi, H. Kawamura, and Y. Toba, "Fine structure of laboratory wind-wave surfaces studied using an optical method," *Boundary Layer Meteorol.* **39**, 133 (1987).

⁵M. S. Longuet-Higgins, "Capillary rollers and bores," *J. Fluid Mech.* **240**, 659 (1992).

⁶B. Jähne and K. Riemer, "Two-dimensional wave number spectra of small scale surface water waves," *J. Geophys. Res.* **95**, 11 531 (1990).

⁷X. Zhang and C. Cox, "Measuring the two-dimensional structure of a wavy water surface optically—A surface gradient detector," *Exp. Fluids* **17**, 225 (1994).

⁸X. Zhang, "Capillary-gravity and capillary waves generated in a wind wave tank: observations and theories," *J. Fluid Mech.* **289**, 51 (1995).

⁹J. Klinke and B. Jähne, "Measurements of short ocean waves during the MBL ARI West coast experiment," in *Air-Water Gas Transfer*, edited by B. Jähne and E. C. Monahan (AEON Verlag & Studi, City, 1995), pp. 165–173.

¹⁰M. Perlin, H. Lin, and C.-L. Ting, "On parasitic capillary waves," *J. Fluid Mech.* **255**, 597 (1993).

¹¹M. S. Longuet-Higgins, "Parasitic capillary waves: A direct calculation," *J. Fluid Mech.* **301**, 79 (1995).

¹²M. S. Longuet-Higgins, "The generation of capillary waves by steep gravity waves," *J. Fluid Mech.* **16**, 238 (1963).

¹³G. D. Crapper, "Non-linear capillary waves generated by steep gravity waves," *J. Fluid Mech.* **40**, 149 (1970).

¹⁴L. M. Schwartz and J.-M. Vander-Broek, "Numerical solution of the exact equations for capillary-gravity waves," *J. Fluid Mech.* **95**, 119 (1979).

¹⁵K. D. Ruvinsky, F. I. Feldstein, and G. I. Friedman, "Numerical simulation of the quasi-stationary stage of ripple excitation by steep gravity-capillary waves," *J. Fluid Mech.* **230**, 339 (1991).

¹⁶G. B. Whitham, *Linear and Nonlinear Waves* (Wiley, New York, 1974).

- ¹⁷A. V. Fedorov and W. K. Melville, "Nonlinear gravity-capillary waves with forcing and dissipation," *J. Fluid Mech.* **354**, 1 (1998).
- ¹⁸M. J. Lighthill, *Waves in Fluids* (Cambridge University Press, Cambridge, 1978).
- ¹⁹L. D. Landau and E. M. Lifshitz, *Fluid Mechanics* (Pergamon, New York, 1987).
- ²⁰B. Chen and P. G. Saffman, "Steady gravity-capillary waves on deep water. 2," *Stud. Appl. Math.* **62**, 95 (1980).
- ²¹X. Zhang, "A study of capillary and capillary-gravity wind waves: their structures, distributions, and energy balances," Ph.D thesis, Scripps Institution of Oceanography, UCSD, 1993.
- ²²P. A. Lange, B. Jähne, J. Tschiersch, and J. Ilmberger, "Comparison between an amplitude-measuring wire and a slope-measuring laser water wave gauge," *Rev. Sci. Instrum.* **53**, 651 (1982).
- ²³J. Zhang and W. K. Melville, "Three-dimensional instabilities of nonlinear gravity-capillary waves," *J. Fluid Mech.* **174**, 187 (1987).
- ²⁴M. A. Donelan and W. J. Pierson, "Radar scattering and equilibrium ranges in wind-generated waves with application to scatterometry," *J. Geophys. Res.* **92**, 4971 (1987).
- ²⁵K. M. Watson and S. B. Buchsbaum, "Interaction of capillary waves with longer waves. Part 1," *J. Fluid Mech.* **321**, 87 (1996).